Dual-Behavior Resonator-Based Fully Reconfigurable Input Reflectionless Bandpass Filters

Roberto Gómez-García, *Senior Member, IEEE*, José-María Muñoz-Ferreras, *Member, IEEE*, and Dimitra Psychogiou, *Member, IEEE*

***Abstract*— A class of input reflectionless dual-behavior resonator (DBR)-based bandpass filters (BPFs) with reconfigurable center frequency, bandwidth, out-of-band attenuation, and intrinsic switching-off capabilities is reported. They exploit a complementary-duplexer approach, in which the resistively terminated bandstop-filter (BSF) channel dissipates the RF input signal energy that is not transmitted by the main BPF channel in its out-of-band region. Spectral reconfiguration is realized through the synchronous tuning of the counterpart resonators in the DBR-based BPF and BSF channels—i.e., without variable couplings—which results in a dynamic transmission-zero (TZ) reallocation process. The theoretical analysis of the first-order section and design examples for higher order schemes are presented. Furthermore, for experimental-validation purposes, a microstrip prototype that can be tuned within the frequency range 1.3–2 GHz is manufactured and characterized.**

***Index Terms*— Absorptive filter, bandpass filter (BPF), complementary duplexer, microstrip filter, planar filter, reconfigurable filter, reflectionless filter, transmission zero (TZ), tunable filter.**

I. Introduction

THE design of RF reflectionless or absorptive bandpass filters (BPFs) is recently attracting a large interest [1]–[4]. These BPFs dissipate within their volume, the nontransmitted RF input signal energy in their stopbands, instead of reflecting it back to the source. Thus, undesired RF power reflections that can deteriorate preceding active stages in the RF chain are eliminated [5]. This is carried out without the use of interblock passive or active isolators, which are bulky or increase dc power consumption, as usually needed in RF front ends when more conventional reflective type BPFs are employed.

Some examples of reflectionless single and multiband BPFs with single-ended and differential-mode operation can be found in [1]–[3]. However, they exhibit a frequency static transfer function. In [4], input reflectionless BPFs with spectral adaptivity were described. Nevertheless, their tunability is limited to center frequency control except for cascades of BPF and notch-type units that allow higher reconfiguration levels at the expense of larger circuit size and in-band insertion loss.

In this letter, fully adaptive input reflectionless BPFs are presented. They exploit a complementary duplexer approach with a dual behavior resonator (DBR)-based BPF channel and its resistively terminated bandstop-filter (BSF) counterpart to absorb the out-of-band RF-signal-power reflections from the former. Thus, by synchronously tuning the counterpart resonators in both channels, reconfiguration in terms of center frequency, bandwidth, stopbands, and intrinsic switching-off capabilities are obtained. To the best of the authors' knowledge, this is the first reflectionless BPF with multiple levels of transfer function adaptivity that is achieved by incorporating tunable DBRs [6]–[8] in the BPF and BSF channels of a reflectionless BPF cell. Hence, this letter demonstrates the extrapolation of the reflective type fully tunable DBR-based BPF concept in [7] and [8] to input reflectionless realizations under the design philosophy in [4].

The rest of this letter is organized as follows: in Section II, the theoretical foundations of the first-order DBR-based input reflectionless BPF section are described. Moreover, higher order design examples are presented. In Section III, a proof-of-concept microstrip prototype with reconfiguration within the band 1.3–2 GHz is developed and tested. Finally, the main concluding remarks of this letter are set out in Section IV.

II. Theoretical Foundations

A. First-Order Section

The coupling–routing diagram of the proposed first-order DBR-based input reflectionless BPF section is depicted in Fig. 1. It results from the basic first-order input reflectionless BPF section without transmission zeros (TZs) that was presented in [4] after applying the normalized frequency transformation in Fig. 1. Thus, a bandpass response with lower and upper TZs at Ω_{z1} and Ω_{z2} that define a normalized passband centered at Ω_0 with 3-dB cutoff frequencies at $\Omega_{c1}^{3\text{dB}}$ and $\Omega_{c2}^{3\text{dB}}$ is obtained. The formulas for these frequencies are as follows:

$$\Omega_0 = \frac{\alpha_1^2\Omega_{z2} + \alpha_2^2\Omega_{z1}}{\alpha_1^2 + \alpha_2^2} \qquad \Omega_{c1}^{3\text{dB}} = \frac{b - \sqrt{b^2 - 4ac_1}}{2a} \tag{1}$$

$$\begin{aligned} \Omega_{c2}^{3\text{dB}} &= \Omega_{z1} + \Omega_{z2} + \frac{b - \sqrt{b^2 - 4ac_2}}{2a} \\ a &= K_A^2 \quad b = \alpha_1^2 + \alpha_2^2 + K_A^2(\Omega_{z1} + \Omega_{z2}) \\ c_1 &= \alpha_1^2\Omega_{z2} + \alpha_2^2\Omega_{z1} + K_A^2\Omega_{z1}\Omega_{z2} \\ c_2 &= \alpha_1^2\Omega_{z1} + \alpha_2^2\Omega_{z2} + K_A^2\Omega_{z1}\Omega_{z2}. \end{aligned} \tag{2}$$

These formulas reveal that the variation of Ω_{z1} and Ω_{z2}—i.e., tuning of the natural frequencies of the DBR

Manuscript received September 2, 2018; revised October 28, 2018; accepted November 26, 2018. Date of publication December 21, 2018; date of current version January 8, 2019. This work was supported in part by the Spanish Ministry of Economy and Competitiveness under Project TEC2017-82398-R and in part by the National Science Foundation under Award 1731956. *(Corresponding author: Roberto Gómez-García.)*

R. Gómez-García and J.-M. Muñoz-Ferreras are with the Department of Signal Theory and Communications, Polytechnic School, University of Alcalá, 28871 Alcalá de Henares, Spain (e-mail: roberto.gomez.garcia@ieee.org; jm.munoz@uah.es).

D. Psychogiou is with the Department of Electrical, Computer, and Energy Engineering, University of Colorado Boulder, Boulder, CO 80309 USA (e-mail: dimitra.psychogiou@colorado.edu).

Color versions of one or more of the figures in this paper are available online at http://ieeexplore.ieee.org.

Digital Object Identifier 10.1109/LMWC.2018.2884151

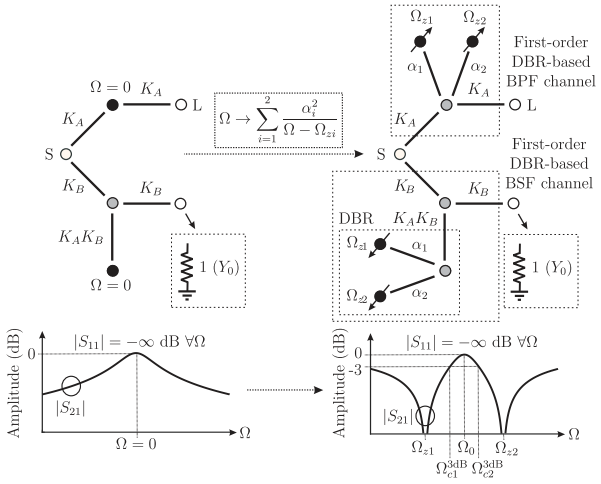

Fig. 1. Normalized coupling routing diagram and conceptual transfer function of the proposed first-order DBR-based input reflectionless BPF section [black circles with arrows: tunable resonating nodes; gray circles: zero-susceptance NRNs; white circles: unitary source (S), load (L), and loading resistor; continuous lines: couplings; $Y_0 = 1/Z_0$: reference admittance for normalization; and Ω: normalized frequency].

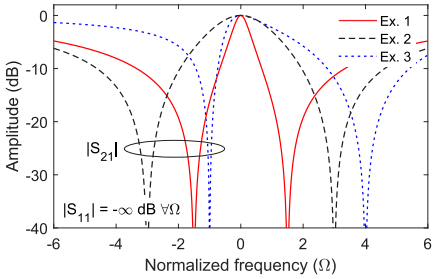

Fig. 2. Example theoretical power transmission responses ($|S_{21}|$) of the first-order DBR-based input reflectionless BPF section in Fig. 1 (example 1: $\Omega_{z1} = -1.5$, $\Omega_{z2} = 1.5$, $\alpha_1 = 2$, and $\alpha_2 = 2$; example 2: $\Omega_{z1} = -3$, $\Omega_{z2} = 3$, $\alpha_1 = 2$, and $\alpha_2 = 2$; example 3: $\Omega_{z1} = -1$, $\Omega_{z2} = 4$, $\alpha_1 = 1$, and $\alpha_2 = 2$; and $K_A = 1$ and $K_B = 1$ in all examples).

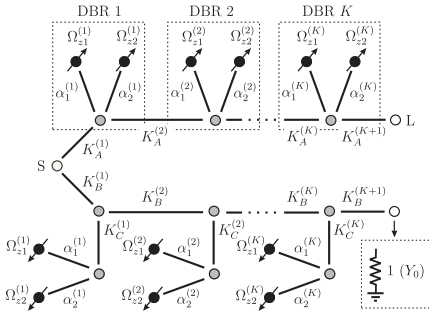

Fig. 3. Normalized coupling-routing diagram of the proposed Kth-order DBR-based input reflectionless BPF.

nodes—allows to control the passband center frequency and bandwidth through Ω_0, $\Omega_{c1}^{3\text{dB}}$, and $\Omega_{c2}^{3\text{dB}}$. Moreover, the perfect input reflectionless behavior inherent to the complementary duplexer approach in Fig. 1 is always maintained. This is verified in Fig. 2, which shows various example theoretical transfer functions with symmetrical and asymmetrical TZs around $\Omega_0 = 0$.

B. Higher Order Designs

The first-order input reflectionless DBR-based BPF section in Fig. 1 can be scaled to higher order designs for increased-selectivity realizations. Fig. 3 represents its Kth-order BPF coupling-routing diagram, in which the

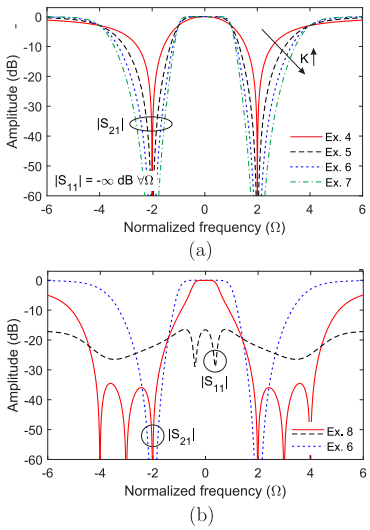

Fig. 4. Example theoretical power transmission responses ($|S_{21}|$) of the Kth-order DBR-based input reflectionless BPF in Fig. 3 (a) Example 4 ($K = 1$): $K_A = 0.8180$, and $K_B = 1$; example 5 ($K = 2$): $K_A^{(1)} = 0.6870$, $K_A^{(2)} = 0.6675$, $K_A^{(3)} = 0.9716$, $K_B^{(1)} = 1$, $K_B^{(2)} = 1$, $K_B^{(3)} = 1$, $K_C^{(1)} = 0.9716$, and $K_C^{(2)} = 0.6870$; example 6 ($K = 3$): $K_A^{(1)} = 0.6674$, $K_A^{(2)} = 0.4725$, $K_A^{(3)} = 0.8183$, $K_A^{(4)} = 1.1560$, $K_B^{(1)} = 1$, $K_B^{(2)} = 1$, $K_B^{(3)} = 1$, $K_B^{(4)} = 1$, $K_C^{(1)} = 1.0011$, $K_C^{(2)} = 0.9439$, and $K_C^{(3)} = 0.5780$; and example 7 ($K = 4$): $K_A^{(1)} = 0.6598$, $K_A^{(2)} = 0.4289$, $K_A^{(3)} = 0.5101$, $K_A^{(4)} = 1.0355$, $K_A^{(5)} = 1.3196$, $K_B^{(1)} = 1$, $K_B^{(2)} = 1$, $K_B^{(3)} = 1$, $K_B^{(4)} = 1$, $K_B^{(5)} = 1$, $K_C^{(1)} = 1.0100$, $K_C^{(2)} = 1.0252$, $K_C^{(3)} = 0.8493$, and $K_C^{(4)} = 0.5050$ ($\Omega_{z1}^{(i)} = -2$, $\Omega_{z2}^{(i)} = 2$, $\alpha_1^{(i)} = 1$, and $\alpha_2^{(i)} = 1$ for $i \in \{1, 2, 3, 4\}$ and all examples). (b) Example 8 ($K = 3$): $K_A^{(1)} = 0.6560$, $K_A^{(2)} = 0.4058$, $K_A^{(3)} = 0.8477$, $K_A^{(4)} = 1.1819$, $K_B^{(1)} = 1.0171$, $K_B^{(2)} = 1.5046$, $K_B^{(3)} = 1.2590$, $K_B^{(4)} = 0.8156$, $K_C^{(1)} = 0.8133$, $K_C^{(2)} = 0.7559$, $K_C^{(3)} = 0.1346$, $\Omega_{z1}^{(1)} = -2$, $\Omega_{z1}^{(2)} = -3$, $\Omega_{z1}^{(3)} = -4$, $\Omega_{z2}^{(1)} = 2$, $\Omega_{z2}^{(2)} = 3$, $\Omega_{z2}^{(3)} = 4$, $\alpha_1^{(1)} = 1.3134$, $\alpha_1^{(2)} = 1.2712$, $\alpha_1^{(3)} = 1.1708$, $\alpha_2^{(1)} = 1.3134$, $\alpha_2^{(2)} = 1.2712$, and $\alpha_2^{(3)} = 1.1708$.

first-order DBR-based BPF and BSF channels are substituted by their Kth-order counterparts. Illustrative frequency responses for the circuit architecture in Fig. 3 are depicted in Fig. 4, in which two distinct cases are analyzed.

1) For identical DBRs, perfectly zero input power reflection can be attained. This is verified in Fig. 4(a), where different order examples with the same 3-dB normalized bandwidth and fully reflectionless behavior at the input are shown. As can be seen, as the order increases, higher selectivity and out-of-band rejection levels are obtained.
2) For dissimilar DBRs exhibiting TZs at different spectral locations, a perfect input reflectionless behavior may not be feasible. Nevertheless, input quasi-reflectionless capabilities can be realized. This is validated in Fig. 4(b), which compares the third-order example in Fig. 4(a) with another one in which the TZs are located at distinct positions. As observed, wider stopbands can be synthesized for dissimilar DBRs but at the expense of lower selectivity and nonzero input power reflection.

III. Experimental Results

To validate the practical viability of the conceived input reflectionless fully reconfigurable BPF, a second-order microstrip prototype with controllable TZs has been built and tested. It was designed for a 50-Ω impedance level and for being spectrally adaptive in the frequency band 1.3–2 GHz.

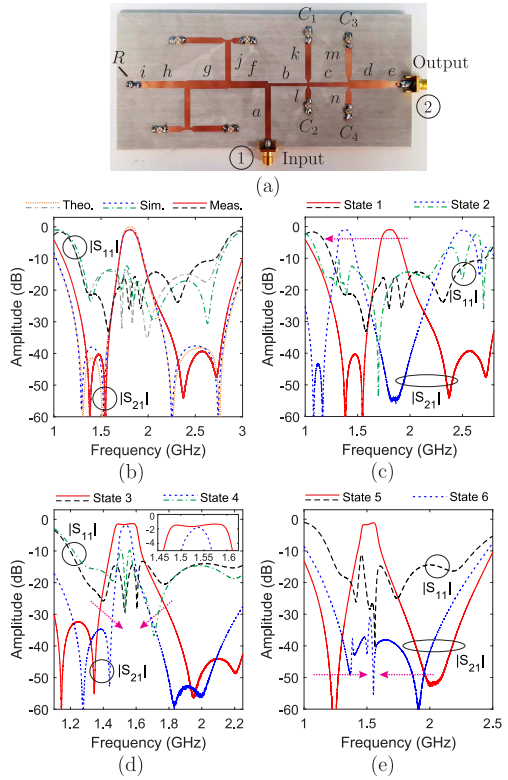

Fig. 5. Manufactured fully reconfigurable input reflectionless BPF prototype (circuit design variables where Z stands for characteristic impedance and θ for electrical length at 2 GHz: $Z_b = 75\ \Omega$, $\theta_b = 90^o$, $Z_c = 60\ \Omega$, $\theta_c = 90^o$, $Z_d = 40\ \Omega$, $\theta_d = 90^o$, $Z_f = 42\ \Omega$, $\theta_f = 90^o$, $Z_g = 40\ \Omega$, $\theta_g = 90^o$, $Z_h = 45\ \Omega$, $\theta_h = 90^o$, $Z_j = 52\ \Omega$, $\theta_j = 90^o$, $Z_k = 50\ \Omega$, $\theta_k = 105^o$, $Z_l = 50\ \Omega$, $\theta_l = 41.1^o$, $Z_m = 50\ \Omega$, $\theta_m = 91.3^o$, $Z_n = 50\ \Omega$, and $\theta_n = 53.8^o$; physical dimensions in mm where w stands for width and l length: $w_a = 3.5$, $l_a = 35.6$, $w_b = 1.7$, $l_b = 21.8$, $w_c = 2.6$, $l_c = 23.1$, $w_d = 4.9$, $l_d = 22.5$, $w_e = 3.5$, $l_e = 15$, $w_f = 4.1$, $l_f = 20.2$, $w_g = 4.9$, $l_g = 20.4$, $w_h = 4.1$, $l_h = 22.1$, $w_i = 3.5$, $l_i = 5$, $w_j = 3.3$, $l_j = 22.9$, $w_k = 3.5$, $l_k = 24.7$, $w_l = 3.5$, $l_l = 7.7$, $w_m = 3.5$, $l_m = 19.6$, $w_n = 3.5$, $l_n = 9.9$, and 2-mm taper length for the resonating lines). (a) Photograph. (b) Theoretical, simulated, and measured power transmission ($|S_{21}|$) and input reflection ($|S_{11}|$) parameters for one example state. (c) Measured center frequency tuning. (d) Measured bandwidth tuning. (e) Measured states with pairs of lower and upper TZs at the same locations and intrinsic switching-off.

In this circuit, the admittance inverters between nonresonating nodes (NRNs) and between NRNs and the source, load, and loading resistor were implemented as quarter wavelength at 2-GHz transmission line segments. The sets shaped by the tunable resonating nodes and adjacent admittance inverters were realized as capacitively loaded quarter-wavelength stubs that produce TZs at 1.47, 1.65, 2.54, and 3.11 GHz—2-GHz passband center frequency—for the lower value of the capacitance variation ranges. For manufacturing, a RO4003C microstrip substrate with the following characteristics was used: relative dielectric permittivity $\varepsilon_r = 3.38$ (± 0.05), dielectric thickness $H = 1.524$ mm, metal thickness $t = 17.8\ \mu$m, and dielectric loss tangent $\tan(\delta_D) = 0.0027$. A 50-Ω resistor from Panasonic and 0.5–2.5-pF mechanically adjustable thin-trim trimmer capacitors from Johanson Manufacturing were employed for tuning, whose ground connections at one edge were realized by means of 1-mm-diameter metallic via holes.

A photograph of the developed prototype is shown in Fig. 5(a). Its theoretical, simulated—with AWR Microwave Office—and measured—with an Agilent-E8361A network analyzer—power transmission and input reflection parameters for one example state are depicted in Fig. 5(b). As can be seen, a fairly close agreement between simulated and measured results is obtained. In this measured state, the center frequency is 1.81 GHz, the 3-dB absolute bandwidth is 160 MHz—i.e., 8.8% in relative terms—the minimum in-band power insertion loss level is 0.96 dB, and the minimum input power matching levels are 15.7 and 10 dB within the 3-dB bandwidth and the 1.252–2.714-GHz band, respectively. The reconfiguration capabilities of this BPF prototype are validated in Fig. 5(c)–(e) while preserving the input reflectionless behavior. This is done by properly reallocating the TZs in the BPF channel as in [6] and [8], and by synchronously tuning the resonators of the BSF channel to absorb the RF input signal power reflections. Fig. 5(c) shows center frequency tuning from 1.37 to 1.81 GHz—i.e., 1.32:1 center frequency tuning ratio—whereas Fig. 5(d) proves 3-dB bandwidth control centered at 1.55 GHz from 145 to 65 MHz—i.e., 2.23:1 bandwidth-tuning ratio—with passband-amplitude flattening for the wideband state. Finally, Fig. 5(e) depicts two different measured states as follows: 1) pairs of lower and upper TZs at the same frequencies for close-to-passband selectivity enhancement at the expense of narrower stopbands and 2) intrinsic-switching-off by detuning the resonators with 20-dB minimum power isolation in the band 1.152–2.279 GHz.

IV. Conclusion

Input reflectionless fully reconfigurable BPFs composed of DBR-based complementary duplexers have been presented. They can be reconfigured in terms of center frequency, bandwidth, and out-of-band TZs and feature passband-intrinsic-switching-off capabilities. Their control is exclusively realized by varying the natural frequencies of the resonators—i.e., without variable admittance inverters and RF switches—through dynamic TZ reallocation. The theoretical operational foundations of this fully adaptive input reflectionless BPF approach have been presented. Furthermore, a proof-of-concept microstrip prototype with spectral reconfiguration in the band 1.3–2 GHz has been constructed and characterized. To the best of the authors' knowledge, it features the highest levels of spectral agility ever reported for reflectionless BPFs.

References

[1] A. C. Guyette, I. C. Hunter, and R. D. Pollard, "Design of absorptive microwave filters using allpass networks in a parallel-cascade configuration," in *IEEE MTT-S Int. Microw. Symp. Dig.*, Boston, MA, USA, Jun. 2009, pp. 733–736.

[2] M. A. Morgan and T. A. Boyd, "Theoretical and experimental study of a new class of reflectionless filter," *IEEE Trans. Microw. Theory Techn.*, vol. 59, no. 5, pp. 1214–1221, May 2011.

[3] R. Gómez-García, J.-M. Muñoz-Ferreras, W. Feng, and D. Psychogiou, "Balanced symmetrical quasi-reflectionless single-and dual-band bandpass planar filters," *IEEE Microw. Wireless Compon. Lett.*, vol. 28, no. 9, pp. 798–800, Sep. 2018.

[4] D. Psychogiou and R. Gómez-García, "Reflectionless adaptive RF filters: Bandpass, bandstop, and cascade designs," *IEEE Trans. Microw. Theory Techn.*, vol. 65, no. 11, pp. 4593–4605, Nov. 2017.

[5] Mini-Circuits, Brooklyn, N.Y., "Reflectionless filters improve linearity and dynamic range," *Microw. J.*, vol. 58, no. 8, pp. 42–50, Aug. 2015.

[6] C. Quendo, E. Rius, and C. Person, "Narrow bandpass filters using dual-behavior resonators," *IEEE Trans. Microw. Theory Techn.*, vol. 51, no. 3, pp. 734–743, Mar. 2003.

[7] E. Fourn *et al.*, "Bandwidth and central frequency control on tunable bandpass filter by using MEMS cantilevers," in *IEEE MTT-S Int. Microw. Symp. Dig.*, Philadelphia, PA, USA, Jun. 2003, pp. 523–526.

[8] D. Psychogiou, R. Gómez-García, and D. Peroulis, "Tune-all RF planar duplexers with intrinsically switched channels," *IEEE Microw. Wireless Compon. Lett.*, vol. 27, no. 4, pp. 350–352, Apr. 2017.